Electronic Supplementary Material (ESI) for RSC Advances.

A microfluidic neuronal platform for neuron axotomy and controlled regenerative studies

Ziqiu Tong, Miriam Segura-Feliu, Oscar Seira, Antoni Homs-Corbera, José Antonio Del Río, and Josep Samitier

Electronic supplemental information

Supp. Fig 1. Characterization of axotomy process on substrate coating. The axotomy chips were coated with FITC-L-Lysine overnight. Fluorescent images were taken before (a) and after (b) passing air bubble through the axotomy channel. Line profiles were drawn across the axotomy channel to determine fluorescence intensity differences before (c) and after (d) axotomy. a1, a2, b1, and b2 indicate the positions of the edges of the axotomy channels. Scale bars = 50 µm.

Supp. Fig 2. Axotomy chips showing width and distance control. (a) Schematic representation of axotomy chips indicating control over the width of axotomy channel. Photomicrographs showing cortical neurons (DIV 7) extending axons over axotomy channels with widths of (b) 30 µm, (c) 50 µm, and (d) 100 µm. (e) Schematic drawing shows the position of axotomy channel relative to the culture chamber area. Photomicrographs showing the axotomy channels are positioned (f) 100 µm, (g) 250 µm, and (h) 500 µm away from the culture chamber.

Supp. Fig 3. Overall characterization of cortical neurons on chip. (a) Stitched panels of photomicrographs indicating the axons growing inside a total of 100 microchannels. (b) After 10 DIV, axons could extend up to 2 mm in length in our culture chip. (c) High resolution photomicrographs show the axons growing inside the axotomy channel and (d) inside the microchannel. Scale bars = 10 µm.

Supp. Fig 4. Introduction of a non-neuronal cell population inside axotomy channel. a) Schematic representation of how second cell population was introduced inside the axotomy channel. b) Calcein AM stained fluorescent image of axons and TEG3 cell inside the axotomy channel. c) The bright field image of axons and TEG3 cells. Scale bars = 50 µm.

Video 1. Mechanical vacuum aspiration via a syringe pump. Inlet well (Ø = 3 mm) was emptied and the outlet well (Ø = 1 mm) was connected to a syringe pump at a withdrawal rate of 3 µL/min. After detachment of the connection tubing, the axotomy channel was automatically filled.

Vídeo 2. Fluorescent beads (Ø = 0.75 µm) were added to the medium of the inlet to monitor the flow behavior of the axotomy channel. Syringe pump was used to withdraw the liquid at a flow rate of 3 µL/min. The fluid flows mainly in a straight profile with limited flow through the microchannels.

Vídeo 3. Polybead® polystyrene blue dyed microsphere (Ø = 3 µm) was used to monitor the flow behavior of the axotomy channel when manually aspirating via a micropipette of P20.

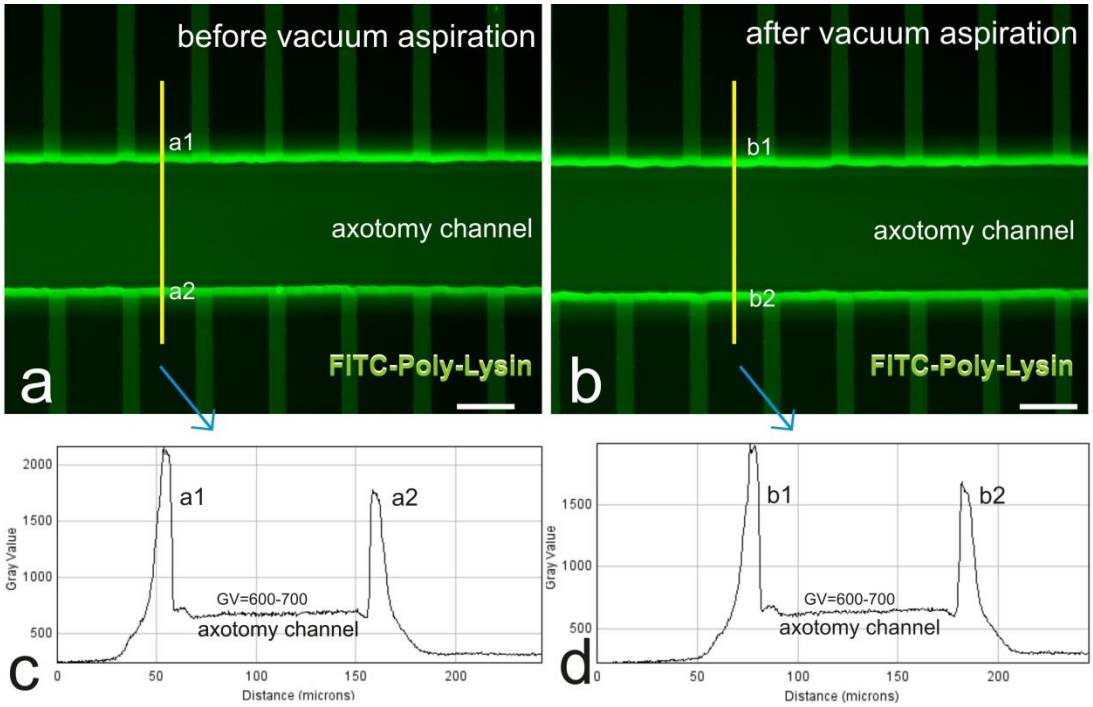

Suppl figure 1

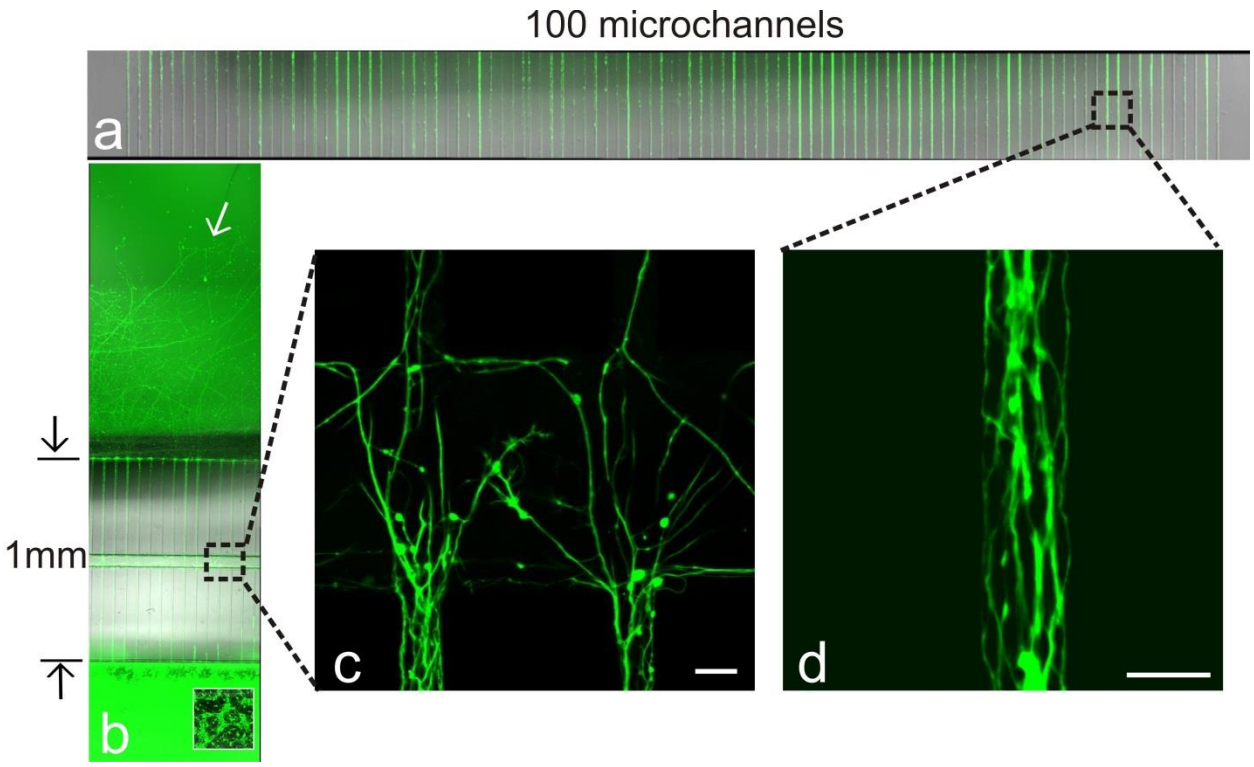

Suppl figure 2

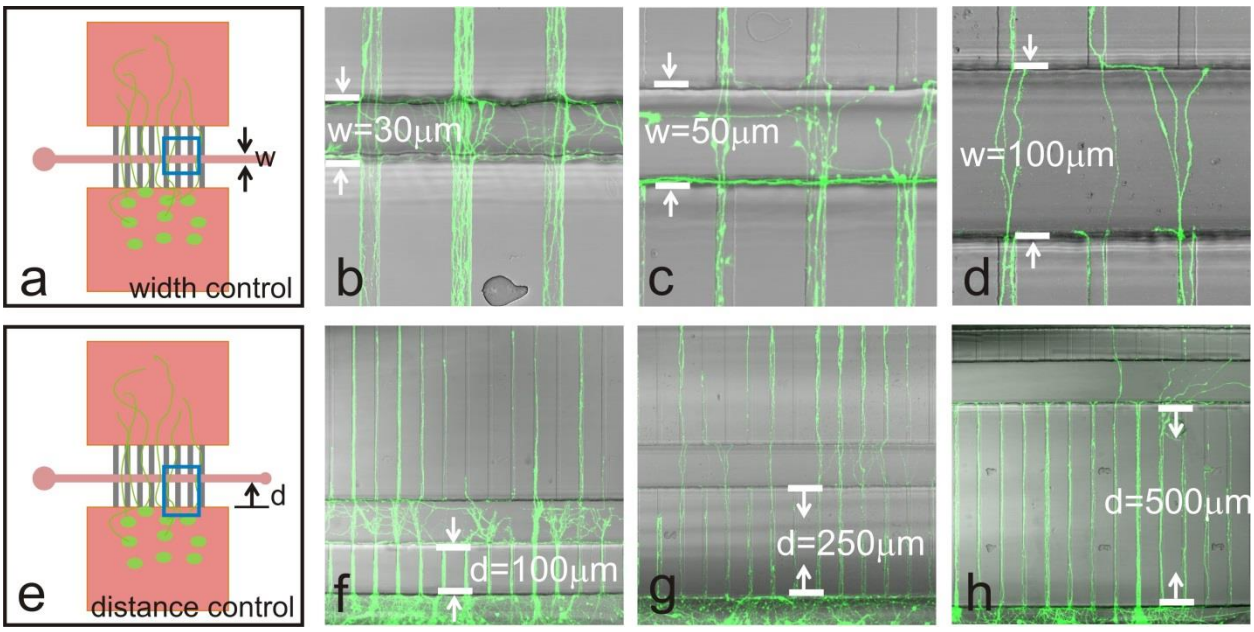

Suppl figure 3

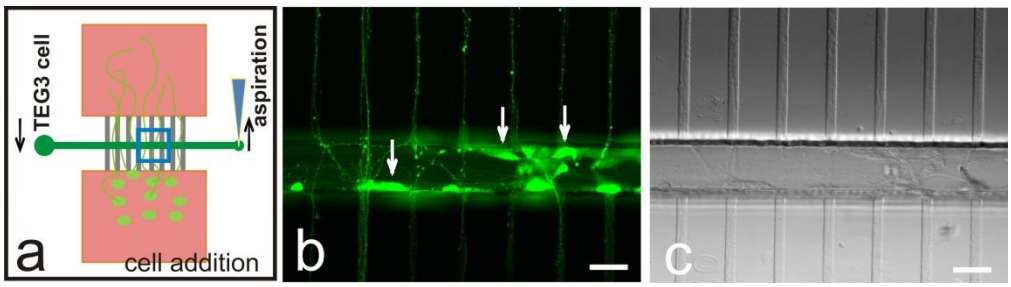

Suppl figure 4

Device Fluidic Model Electronic Supplementary Information

A microfluidic simplified model was done based in circuits theory equivalents (Figure S1) on top of the regular COMSOL Multiphysics® V5.0 (COMSOL Ltd) simulations to verify the lab-on-a-chip behaviour.

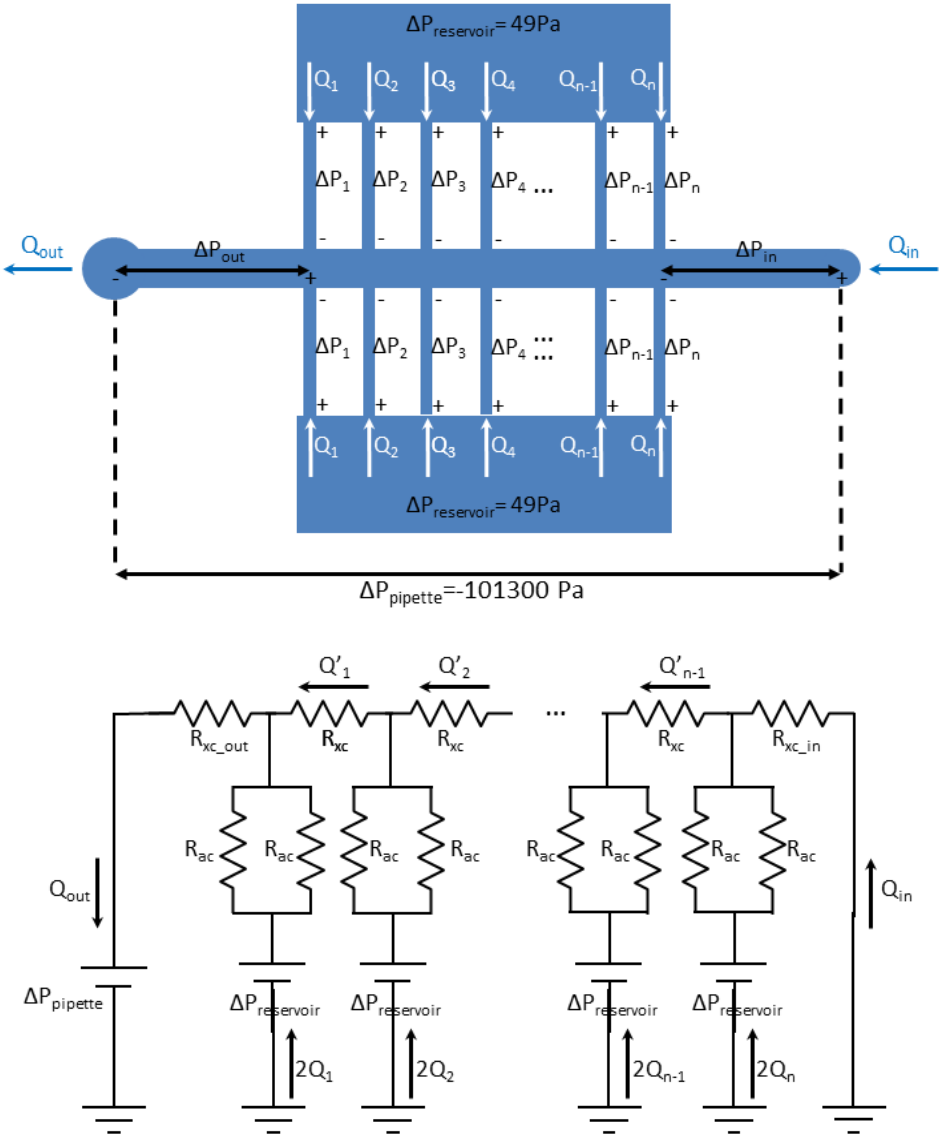

Figure S1. Simplified hydraulic model based on circuits theory. In the model, R_{cx_out}, the subsequent R_{cx} values, and R_{cx_in}, will change while air flows in the circuit displacing the buffer.

The values for $\Delta P_{pipette}$ and $\Delta P_{reservoir}$ were estimated to be -101300 Pa and 49 Pa respectively. The pressure at the reservoirs was estimated taking into account a height of 5 mm in both reservoirs at equilibrium.

The values for the different hydrodynamic resistances (R_H) were estimated using the general rectangular cross-section equation:

$$R_H = \frac{12\eta l}{wh^3}\left[1 - \frac{h}{w}\left(\frac{192}{\pi^5}\sum_{i=1}^{\infty}\frac{1}{i^5}\tanh\left(\frac{i\pi w}{2h}\right)\right)\right]^{-1}$$

Where w, h, and l correspond to the width, height, and length of the microchannels section, and η is the viscosity ($1.0x10^{-3}$ and $1.9x10^{-5}$ Pa·s, for water and air, at 20°C, respectively).

Results obtained when considering the system filled with buffer solution, as it happens when the negative pressure is initially applied, and with air, as it happens when the solution in the axotomy channel finishes, can be seen in Table S1 when the device with a 30 µm wide axotomy channel is used. To calculate the forces a density of 1000 Kg/m^3 was considered for the axon.

		Buffer	**Air**
Q_{in}	(µl/min)	$3.37x10^{2}$	$1.81x10^{4}$
Q_n	(µl/min)	$5.33x10^{-2}$	$5.44x10^{-2}$
Q'_{n-1}	(µl/min)	$3.37x10^{2}$	$1.81x10^{4}$
Q'_1	(µl/min)	$3.53x10^{2}$	$1.82x10^{4}$
Q_1	(µl/min)	$1.07x10^{-1}$	$1.08x10^{-1}$
Q_{out}	(µl/min)	$3.53x10^{2}$	$1.82x10^{4}$
Δv(Qin→Q'n-1)	(m/s)	$9.52x10^{-4}$	$1.43x10^{-3}$
Δv(Qn→Qin)	(m/s)	2.64	$1.44x10^{2}$
Δv(Qn→Q'n-1)	(m/s)	2.64	$1.44x10^{2}$
Δv(Q1→Q'1)	(m/s)	2.73	$1.44x10^{2}$
Δv(Q1→Qout)	(m/s)	2.73	$1.44x10^{2}$
Δv(Q'1→Qout)	(m/s)	$1.90x10^{-3}$	$2.86x10^{-3}$
F(Qin→Q'n-1)	(N)	$6.01x10^{-12}$	$4.85x10^{-10}$
F(Qn→Qin)	(N)	$> 8.22x10^{-9}$	$> 2.44x10^{-5}$
F(Qn→Q'n-1)	(N)	$> 8.23x10^{-9}$	$> 2.44x10^{-5}$
F(Q1→Q'1)	(N)	$> 8.78x10^{-9}$	$> 2.44x10^{-5}$
F(Q1→Qout)	(N)	$> 8.80x10^{-9}$	$> 2.44x10^{-5}$
F(Q'1→Qout)	(N)	$1.26x10^{-11}$	$9.70x10^{-10}$

Table S1. Example of the values obtained through the mathematical model (supposing an axotomy channel of 30x70 μm^2 cross-section) for flow, acceleration, and force suffered by the axon at the flow channels intersections near the inlet and the outlet of the axotomy channel.

When equilibrium is altered by applying a negative pressure, due to the pipette action, flow in the axon channels is some orders of magnitude slower than the flow in the axotomy channel. Furthermore, the magnitude of the flow in the axon channels remains quite stable when the buffer is substituted by air, during the aspiration procedure, while it changes dramatically (2 orders of magnitude) in the axotomy channel (Table S1). This whole effect creates a clean cut of the axons at the interface of the flows of both channels while preserving the cells and the axon portions at the reservoirs and axon channels.

The principle of operation of the microfluidic axotomizing device relies on the effect of the accelerations experimented by the portion of the axons which cross the axotomy channel. The flow through the axotomy channel is accelerated in each microchannel producing a perpendicular force resulting from this drag. Furthermore, and most importantly, as seen also in the model, a strong shear stress, and sudden velocity change, affects the portion of the axon which is caught just between each slow flow axon channel and the fast flow axotomy channel.

This is due the large differences on hydraulic resistance between the axon channels and the axotomy channel. These effects become more dramatic as the central axotomy channel fluidic resistance is lowered, by increasing its cross section or changing its crossing liquid properties, or as the axon channels

are thinned or elongated. The sudden appearance of air in the central axotomy channel lowers its hydraulic resistance producing an increase of the forces tending to break the axon.

In the Figure S2 below, the dramatic change in velocity experimented at the microchannels intersection can be seen when visualizing the COMSOL Multiphysics model of the 30x70 μm^2 cross-section axotomy channel version of the microfluidic chip. On the other hand, due to the relative small contribution of flow from the axon channels to the axotomy channels, the increase of the central channel, velocity at each intersection, is not easily appreciated while completely filled with buffer. However, when the axotomy channel is freed from buffer, while being substituted by air, the increase of the velocity in the axotomy channel is well appreciated while the axon channels velocity is practically not affected. It is interesting to notice that the more complex COMSOL model suggests that, due to the parabolic profile of the flow, as the air front approaches the axon channels, it experiments faster velocity changes in the peak of its profile, since it is affected by the acceleration near the axon channel in the first place, while being in the transient from buffer-filled to air-filled axotomy channel.

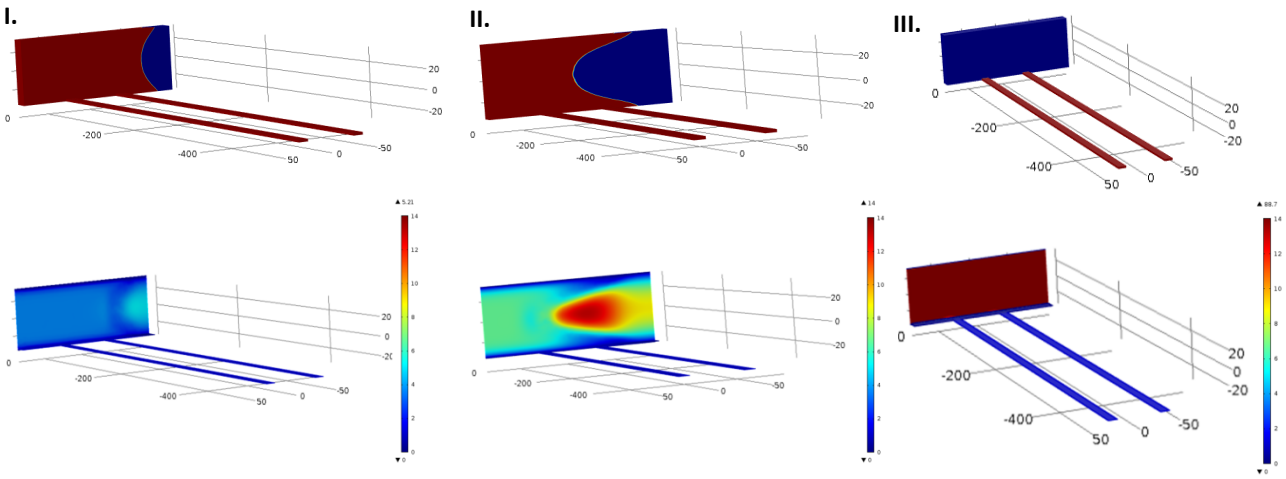

Figure S2. 3 time-frame snapshots of the Comsol Multiphysics, two-phases simplified model (considering the first 2 axon channels section at the inlet side only, and symmetry boundary conditions at the central axis of the axotomy channel). Top row represents the fluid fraction (air is blue while buffer is red) while the bottom shows the ortogonal velocity planes (in m/s) at the middle of the axotomy channel and the axons channels. The 3D dimensions are given in µm. Velocity color scale is always represented between 0 and 14 m/s. **S2.I.** represents the situation when the channel is fulfilled with buffer and air is introduced, due to the pipette aspiration. **S2.II.** corresponds to the situation when air starts crossing the first axon channel. **S2.III.** shows the situation when the axotomy channel has been completely filled with air.